Research Square

Preprints are preliminary reports that have not undergone peer review.
They should not be considered conclusive, used to inform clinical practice,
or referenced by the media as validated information.

REST Promotes Pancreatic Ductal Adenocarcinoma Progression by Inhibiting NOXA1/ROS Pathway-Induced Cell Pyroptosis

chengxu Sui

suichengxu@163.com

The Second Hospital of Dalian Medical University

Jiao Li

Shanghai East Hospital

Ruojie Li

The Second Hospital of Dalian Medical University

Man Li

The Second Hospital of Dalian Medical University https://orcid.org/0000-0003-1672-2190

Research Article

Keywords: pancreatic ductal adenocarcinoma, pyroptosis. REST, NOXA1, GSDMC

Posted Date: May 28th, 2026

DOI: https://doi.org/10.21203/rs.3.rs-9635765/v1

License: This work is licensed under a Creative Commons Attribution 4.0 International License.
Read Full License

Abstract

Inducing alternative programmed cell death is a promising strategy for apoptosis-resistant pancreatic ductal carcinoma (PDAC). The RE-1 silencing transcriptional repressor (REST) has been recognized to govern genesis of embryonic pancreas. Whether REST participates in regulating alternative programmed cell death of PDAC has not been revealed. In this study, we applied immunohistochemistry assays to illustrate the association between REST expression level with PDAC tumor stage and outcome. Role of REST in PDAC progression was valid in transgenic mice PDAC model. Functional analysis was applied to demonstrate the pro-pyroptosis effect of REST in PDAC cells. The regulatory mechanisms through which REST inhibits NOXA1 gene transcription and PDAC cell pyroptosis were also investigated. In this research, we demonstrated that REST expression level was associated with advanced PDAC tumor stage and poor patient prognosis in both our patient cohort and public PDAC cohorts. Through *in vitro* and *in vivo* models, we found that REST promotes PDAC cell proliferation, anchorage spheroid formation, and tumor growth by repressing GSDMC-mediated cell pyroptosis. Mechanistically, REST directly represses NOXA1 gene transcription, thereby increasing ROS production in PDAC cells. Increased ROS activates the death receptor 6 (DR6) and subsequently induces GSDMC/Caspase-8-mediated pyroptosis. Targeting REST expression in transgenetic mice PDAC model repressed tumorigenesis and tumor progression by inducing pyroptosis in PDAC cells. Our research reveals a novel function of REST in regulating PDAC progression by inhibiting ROS-mediated PDAC cell pyroptosis.

Summary

This study investigates the role of REST in pancreatic ductal carcinoma (PDAC), revealing its association with tumor progression and poor prognosis by inhibiting GSDMC-mediated pyroptosis, thus promoting cell proliferation and tumor growth.

1. INTRODUCTION

Pancreatic ductal adenocarcinoma (PDAC) is one of the most lethal cancers worldwide, with a merely 7% 5-year survival rate(1). Approximately 80% of PDAC are diagnosed at the advanced or metastatic stage which are not appropriate for surgical resection(2, 3). Although systemic chemotherapy initially proves effective for these patients, it has been reported that the majority of them develop chemoresistance within several months. This resistance is known to be at least partly driven by antiapoptotic mechanisms(4, 5). Hence, inducing alternative programmed cell death in PDAC, such as necroptosis, ferroptosis, or pyroptosis, would be a promising therapeutic strategy to overcome antiapoptosis-mediated resistance to chemotherapy.

PDAC is believed to originated from pancreatic exocrine acinar cells and trans-differentiated into a more epithelial-like and malignant phenotype(6). During pancreas development, the RE-1 silencing transcriptional repressor (REST) was recognized as an important negative regulator of programmed

differentiation(7). REST was originally identified as a transcriptional repressor that silences neuronal genes by binding to RE-1 elements and recruiting chromatin-modifying enzyme complexes (8, 9). Recent single-cell RNA-seq data showed REST expression in adult ductal cells, but not in acinar or endocrine cells of the pancreas(10, 11), suggesting a potential role in acinar-to-ductal transdifferentiation. However, whether REST participates in PDAC oncogenesis and progression remains unknown.

Pyroptosis is a form of programmed cell death characterized by membrane pore formation, cell swelling and lysis, and release of proinflammatory cytokines (12, 13). While sharing some morphological features with apoptosis and necrosis, pyroptosis is uniquely mediated by caspase-induced cleavage of gasdermin family members(13, 14). Unlike caspase-3 and caspase-7, which are primarily involved in apoptosis, caspase-8 is essential for certain pyroptosis pathways and can cleave IL-1β and IL-18 (15). The release of these proinflammatory cytokines mediates interactions between tumor cells and inflammatory cells within the cancer microenvironment(16). Therefore, specifically inducing pyroptosis in PDAC could both bypass anti-apoptotic mechanisms and trigger antitumor immunity. However, the molecular mechanisms regulating PDAC cell pyroptosis remain largely unexplored.

In the present research, we found that the REST mRNA and protein levels were significantly elevated in PDAC and associated with tumor stage as well as patient survival. REST stimulates PDAC cell proliferation, anchorage spheroid formation, and tumor growth while inhibits PDAC cell pyroptosis. Consequently, we further demonstrated the mechanism through which REST depletion promotes NADPH oxidase activator 1 (NOXA1) expression and elevated intracellular reactive oxygen species (ROS) production. Elevated ROS activates death receptor 6 (DR6) and engage Caspase-8 to cleave gasdermin C(GSDMC), thereby inducing pyroptosis. These findings reveal a previously unrecognized role of REST in regulating PDAC pyroptosis and provide a potential anti-apoptotic therapeutic strategy for PDAC.

2. MATERIAL AND METHODS

2.1Pancreatic tissue microarray (TMA) construction and pathology evaluation

The Benign-PDAC TMA containing benign pancreas and pancreatic ductal tumor samples were retrieved from patients who underwent surgery for PDAC at The Second Affiliated Hospital of Dalian Medical University. This TMA contains tissue cores from 55 patients who had been diagnosed as primary pancreatic ductal tumor and underwent pancreaticoduodenectomy or resection of body and tail of pancreas plus splenectomy. The PDAC-survival TMA was constructed using 186 tissue cores from patients diagnosed with primary PDAC who underwent surgical resection, including pancreaticoduodenectomy or distal pancreatectomy with splenectomy. All patients were prospectively followed up postoperatively for long-term survival analysis. All patients had given informed consent to the protocol that was reviewed and approved by the Dalian Medical University (Certificate #: 2020 No.120). These tissues were flash frozen in liquid nitrogen immediately after surgery and subsequently stored at -80°C. All the resected tissues were identified as PDAC tumor and adjacent normal tissues

through pathological examination. No patients received any anticancer treatments including chemotherapy and radiotherapy before surgery in this study. All samples were classified and staged in accordance with the tumor node metastasis (TNM) classification. Written informed consent was obtained from all patients. The Ethics Committee of The Second Affiliated Hospital of Dalian Medical University approved the use of tissues for this study.

2.2 Immunohistochemistry (IHC) analyses

IHC was performed on TMA using indicated antibodies by Ventana Discovery XT (Ventana) using the DAB MAP kit and scanned by the Leica SCN400 scanner. Staining signals were scored and calculated by the staining intensity (no = 0, low = 1, moderate = 2, and high intensity staining = 3) times percentage of stained cells (0-100%).

2.3 PDAC Mouse model strains

To establish a spontaneous pancreatic cancer model, *Krt19-cre*$^{+}$*Trp53*$^{MT/MT}$*Kras*$^{G12D/+}$ mice were utilized. These mice develop pancreatic intraepithelial neoplasia (PanIN) lesions that progress to invasive pancreatic ductal adenocarcinoma (PDAC) over time. Mice were monitored weekly for weight loss and signs of illness. Tumor progression was confirmed via histopathological analysis of pancreatic tissues at defined timepoints. All procedures were approved by the Institutional Animal Care and Use Committee (IACUC).

The transgenic mice with pancreatic ductal epithelial cell specific knock down *Rest* induced by Doxycycline (DOX) were generated by Cyagen Company (Suzhou, China).

Briefly, the "Krt19 promoter-Kozak-Tet3G-rBG pA-anti[TRE3G promoter-Kozak-EGFP-5' miR-30E/Rest-shRNA/3' miR-30E-WPRE-BGH pA]" cassette will be inserted into H11 locus in *Trp53*$^{MT/MT}$*Kras*$^{G12D/+}$ mice. And the miR30-styled shRNA will be expressed under the control of pancreatic ductal epithelial cel-specific Krt19 promoter by the Tet-on system. The homology arms will be generated by PCR using BAC clone as template. The pups will be genotyped by PCR followed by sequencing analysis confirmation for positive targeting. REST depletion will be induced in vivo by administering proper doxycycline in drinking water or food.

2.4 Cell culture and cell lines

The PDAC cell lines PANC-1 were purchased from ATCC and cultured at 37°C in 5% CO_2 in DMEM Medium containing 10% fetal bovine serum (HyClone). The integrity of PANC-1 cell line was authenticated by STR.

The PANC-1 (CTL) and PANC-1 (REST) cell lines were generated using PANC-1 cells infected with lentivirus bearing sequences encoding control or REST genes, followed by puromycin selection. While PANC-1 (shCTL) and PANC-1 (shREST) cell lines were constructed following similar procedure and underwent puromycin selection. Vectors encoding shRNA targeting REST mRNA were purchased from

Dharmacon. Overexpression or knockdown of REST gene were confirmed by real-time PCR and immunoblotting assays.

2.5 Immunoblotting and real-time PCR

The total protein lysates from the cell were isolated, electrophoresed on SDS polyacrylamide gels, and subsequently blotted onto PVDF membranes. The presence of specific proteins was then revealed using the designated antibodies, details of which are provided in the supplementary table 1. These procedures were conducted with three separate biological samples for replication. Of the triplicate immunoblotting analyses, only a single exemplar result is depicted.

In terms of RNA isolation, total cellular or tissue RNA was extracted using TRIZOL reagent and purified with the mirVana miRNA isolation kit as per the manufacturer's guidelines. To remove any DNA contaminants, deoxyribonuclease was applied to the mRNA extractions. The conversion of mRNA to cDNA was achieved using superscript III (Invitrogen) and random hexamers, following the manufacturer's protocols. Quantitative real-time PCR was then executed on the QuantStudio™7 system employing the FastStart Universal SYBR Green Master mix. For each PCR experiment, measurements were conducted in triplicate across three separate experimental setups. The primers used to amplify target genes are listed in the supplementary table 2

2.6 Immunofluorescence assays

Samples were preserved in 4% paraformaldehyde and made permeable with 0.25% Triton X-100, followed by a blockage step using 1% BSA for 60 minutes at room temperature. Subsequently, the sample sections were treated with the specified primary antibodies, followed by rinses in PBS containing 0.1% Triton X-100, and later tagged with FITC-labeled secondary antibody (diluted 1:1000 in PBS-T with 1% BSA). The visualization of tissues was performed using a Zeiss fluorescent microscope (Carl Zeiss).

2.7 Cell proliferation, invasion and colony formation assays.

Cell proliferation rates were measured by the MTS assays according to the manufacture's protocol and were presented as relative fold change of absorbance at 450nm and normalized to that at the day zero.

The Bromodeoxyuridine (BrdU) label incorporation test was executed as per the guidelines provided by the manufacturer. In a summarized procedure, BrdU solution, diluted at 1:500, was administered to 1×10^4 cells which were then allowed to incubate for a duration of 16 hours. Following this, BrdU incorporation was identified using an anti-BrdU antibody diluted at 1:1000 and a horseradish peroxidase-conjugated secondary antibody. Subsequent to the addition of TMB peroxidase substrate, changes in absorbance at 450nm were measured using a densitometer. The BrdU incorporation rate was expressed as a fold increase in OD450, standardized against the control sample.

The determination of the cell invasion capability utilized transwell assays, carried out as specified by the manufacturer. In a concise process, cells underwent starvation for 16 hours, followed by suspension in

serum-free medium prior to their introduction into Matrigel-coated transwell inserts that had been prehydrated. The lower compartment was filled with DMEM containing 2% FBS. After a 16-hour incubation period, residual cells within the inserts were removed. Cells that had migrated were then fixed in 4% paraformaldehyde and subjected to a 10-minute stain with Hoechst dye (Invitrogen), with imaging subsequently conducted using a Zeiss fluorescent microscope. Each assay was replicated thrice.

For the soft-agar colony forming assessment, approximately 1×10^3 cells were placed within 0.375% soft agar in DMEM supplemented media, atop a layer of 0.75% noble agar, in a triplicated setup and this procedure was repeated twice. Post a growth period of 10 days, colonies exceeding 0.1mm in size were tallied, with an average count calculated from the collected data.

2.8 3D spheroid culture and high throughput screening system

The 3D spheroid culture of PANC-1 cells was performed using GravityPLUS™ Hanging Drop System. On the GravityPLUS™ spheroid culture plate, a 40ul liquid drop containing 2×10^3 PANC-1 cells was used to form the hanging cell suspension drop and the culture medium was replenished every two days. After tumor spheroid formation, these spheroids were then transferred into the GravityTRAP™ culture plates for further experiments. Images of tumor spheroids were captured and the sizes of spheroids were measured using the Imagine-J software.

2.9 Xenograft assay

Every procedure involving animals was conducted in compliance with a protocol, number 20141204, which received approval from the Research Ethics Committee of East China Normal University. Nude mice, aged approximately 4–6 weeks, were utilized in these experiments. About 1×10^5 cells were grown in culture before being subcutaneously injected into the lateral sides of the hind flanks. Tumor development was observed and recorded on a weekly basis, once or twice per week. The formula for determining tumor size was as follows: Tumor volume = Length×$(\text{Width})^2$×0.562.

2.10 Chromatin immunoprecipitation (ChIP)

Chromatin immunoprecipitation assays were performed using MAGnify™ ChIP kit (Invitrogen) according to the manufacture's protocol. The primers used to amplify target region are listed in the supplementary table 2.

2.11 Construction of NOXA1-Luc report vectors and Luciferase reporter assay

The human genomic BAC clone served as the DNA template for amplifying the − 3000 to + 100 region of the NOXA1 gene, using the Platinum Taq DNA Polymerase High Fidelity enzyme (Invitrogen). The amplified PCR product was subsequently inserted into the pGL4.10 firefly luciferase reporter vector to create the NOXA1-Luc reporter construct. Utilizing the wild type NOXA1-Luc reporter as a template, a

mutant version of the NOXA1-Luc reporter was crafted with the aid of a Q5 site-directed mutagenesis kit (Invitrogen). Sanger DNA sequencing was employed to verify the structural accuracy of these reporter vectors.

For the luciferase assays, PANC-1 cells were transfected with the aforementioned Luc-reporter vectors, employing a renilla luciferase vector as an internal standard for control. The measurement of luciferase activity was performed using the luciferin substrate (Promega), following the protocol provided by the manufacturer. The luciferase activity readings were adjusted for transfection efficiency, using the renilla luciferase activity as a baseline for normalization.

2.12 Immunoprecipitation and western blotting

PANC-1 cells were disrupted using a lysis buffer composed of 50 mM Tris (pH = 7.5), 150 mM NaCl, 1 mM EDTA, 1 mM EGTA, 2.5 mM sodium pyrophosphate, 1% Triton X-100, 1 mM phenylmethylsulfonyl fluoride, and a mixture of protease inhibitors on ice. Following this, the lysed cells were treated with specified antibodies at 4°C over a period of 16 hours and then coupled with protein G-Sepharose beads at 4°C for an additional hour. The protein-antibody complexes were then isolated using lysis buffer infused with β-mercaptoethanol and analyzed via western blot.

In examining protein oxidation, both reduced and non-reduced samples were readied, the latter omitting β-mercaptoethanol. Lysed cells were gathered using a 2×SDS loading buffer devoid of β-mercaptoethanol (0.1 M Tris, 20% glycerol, 4% SDS, and 0.02% bromophenol blue). The separation of these samples was conducted through SDS-PAGE, with non-reduced samples undergoing electrophoresis on a gradient gel ranging from 4% to 12%, provided by Sangon Biotech.

2.13 Intracellular ROS levels

To detect the intracellular ROS levels, PANC-1 cells were incubated with 10μM CM-H2DCFDA in serum-free DMEM for 15 minutes at 37°C in the dark and then washed with serum-free DMEM for three times. Then the cells were collected, and ROS levels were analyzed using an FC500 (Beckman) flow cytometer. Mean fluorescence intensity (MFI) was quantified using FlowJo software. For each sample, at least 10,000 viable cells were analyzed. ROS levels were normalized to the control group and expressed as fold change relative to control. Background fluorescence from unstained cells was subtracted from all samples.

2.14 LDH release assay

The CytoTox 96 nonradioactive cytotoxicity assay kit (Promega) were used to detected the LDH released into the culture supernatants during pyroptosis according to the manufacturer’s protocol.

2.15 Cell fraction assays

In the process of isolating the Triton X insoluble fraction, PANC-1 cells underwent lysis using a chilled lysis buffer containing Triton X-100 (50 mM Tris-HCl (pH = 7.5), 150 mM NaCl, 1% Triton X-100, 1 mM phenylmethylsulfonyl fluoride, and a protease inhibitor cocktail), followed by a 15-minute incubation

period on ice. Subsequently, the lysates were subjected to centrifugation at 15,000×g for 30 minutes at a temperature of 4°C, facilitating the collection of the Triton X-100 insoluble fractions. The supernatants were reserved as the Triton X-100 soluble fractions. To clean, the Triton X-100 insoluble fractions were rinsed with lysis buffer, then treated with lysis buffer supplemented with 1% SDS and heated at 60°C. After sonication, these insoluble fractions were further processed for immunoblot analysis.

For membrane fraction assay, cytosolic proteins and membrane proteins were separately extracted by a plasma membrane protein extraction kit (Abcam) according to the manufacturer's protocols. Experiments were repeated in three independent experiments, and one of the representative blots was shown.

2.16 RNA run-on assay and stability assay

Totally 1×10^7 cells were lysed and centrifuged to collect the nuclei. In vitro transcription was carried out in a mixture containing 2.5mM of NTP and biotin-16-UTP mix (Roche) and reaction buffer (10mM of Tris·HCl (pH = 8.0), 5mM of $MgCl_2$, 0.3mM of KCl. The in vitro transcription system was incubated at 30°C for 45 minutes. Biotin-labeled nascent RNA transcripts were precipitated and collected from the in vitro transcription system by streptavidin beads. Purified nascent RNA was used as templates for real-time PCR assays.

2.17 Production and injection of AAV

AAV8-rep/cap-Y-F mutant virus expressing shRNA targeting human or mouse REST was constructed and packaged by HAN Biosciences (Shanghai, China). The viral DNA-containing AAV vector titers were quantified by real-time PCR analysis. A 10-fold dilution series of the control plasmid DNA was used to generate a standard curve to determine the AAV vector genome titer (GC/mL). After viral titration (> 1×10^{13}GC/mL), the AAV was aliquoted and stored at -80°C until used. The mice were randomly grouped before being intravenously administered a single dose of 4×10^{12} vg/kg of AAV8_sh*Rest* or AAV_shCTL (scramble controls) via the tail vein.

2.18 Statistics

All in vitro experiments were performed in at least three independent biological replicates. For animal studies, sample sizes are indicated in the figure legends. For immunoblotting and immunofluorescence, representative images from at least two independent experiments are shown. Statistical analysis was performed by the GraphPad Prism 9.0 software. Differences among groups were compared by one-way ANOVA test. Spearman correlation analysis was used to evaluate the correlation between RISH scores with tumor stage. Survival analysis was performed using the Kaplan-Meier method, and differences between groups were compared using the log-rank test. Patients were stratified into REST-high and REST-low groups based on the median IHC score or mRNA expression z-score. The level of significance was set at $p < 0.05$ as *, $p < 0.01$ as **.

3. RESULTS

3.1 Elevated REST Expression Correlates with PDAC Progression and Poor Prognosis in Human Tissues and Murine Models

To evaluate REST expression in human pancreatic tissues, we analyzed publicly available patient-derived data from the GETx(17), GEO and TCGA databases(18). Genomic profiling of PDAC and normal tissues in the GETx database revealed a statistically significant upregulation of REST mRNA levels in PDAC tumors compared to normal tissues (Fig. 1A). This finding was further validated in independent datasets (datasets GSE62452(19) and GSE71729(20)), which demonstrated a pronounced increase in REST expression in primary PDAC and metastatic tissues relative to benign pancreatic tissues (Fig. 1B). Additionally, analysis of TCGA data indicated that REST mRNA levels were significantly higher in advanced-stage (T3-4) PDAC compared to early-stage (T1-2) tumors (Fig. 1C). Consistent with these observations, RNA-seq and clinical data from TCGA revealed that elevated REST expression was associated with reduced overall and disease-free survival in PDAC patients (Fig. 1D).

We next evaluated REST protein expression using a tissue microarray (TMA) comprising benign and PDAC tissues from 55 patients. Immunohistochemical (IHC) analysis revealed minimal REST expression in normal pancreatic tissues, moderate levels in pancreatic intraepithelial neoplasias (PanINs), and significantly elevated expression in PDAC tissues (Fig. 1E-F). Notably, REST expression was nearly absent in benign tissues but increased progressively with higher tumor stage (Fig. 1G). Furthermore, PDAC tumors with lymph node metastasis exhibited significantly higher REST IHC scores compared to those without metastasis (Fig. 1H). Consistent with the mRNA findings from GTEx and TCGA databases, analysis of a survival TMA (n = 185) demonstrated that high REST expression correlated with shorter disease-free survival compared to low REST-expressing tumors (Fig. 1J). Additionally, REST expression was markedly upregulated in tumor tissues from the *Kras/Trp53* double mutant-driven PDAC transgenic mouse model (Fig. 1K). Collectively, these data demonstrate that elevated REST expression is associated with advanced PDAC progression and worse patient prognosis.

3.2 REST promotes PDAC progression

To investigate the functional role of REST in PDAC progression, we generated PANC-1 cell lines with stable REST overexpression or knockout (Fig. S1A). Functional assays revealed that REST overexpression significantly enhanced cell proliferation, as demonstrated by both MTS and BrdU incorporation assays (Fig. 2A-B). Moreover, REST promoted invasive capacity and increased anchorage-independent colony formation (Fig. 2C-D). Apoptosis assays showed that REST overexpression reduced paclitaxel-induced cytotoxicity, evidenced by decreased LDH release and fewer TUNEL-positive cells (Fig. 2E-F). In a 3D culture model, PANC-1(REST) spheroids exhibited accelerated growth, whereas PANC-1(shREST) spheroids showed growth suppression (Fig. 2G). To validate these findings in vivo, we employed a xenograft model, which demonstrated that REST overexpression promoted tumor growth while REST knockdown inhibited it. IHC analysis further confirmed that REST enhanced Ki-67 expression, indicative of increased proliferative activity (Fig. 2H). Collectively, these results demonstrate that REST drives PDAC progression by stimulating proliferation, inhibiting apoptosis, and promoting tumor growth.

To further examine the oncogenic role of REST, we developed a *Trp53* and *Kras* double mutant-driven PDAC mouse model with pancreas-specific REST deletion upon DOX treatment (Fig. 2I and S1B). REST knockout significantly extended the tumor-free survival of *Krt19-cre^{+}Trp53$^{MT/MT}$Kras$^{G12D/+}$* mice (Fig. 2I). Moreover, *Krt19-cre^{+}Trp53$^{MT/MT}$Kras$^{G12D/+}$;Rest$^{-/-}$* mice exhibited reduced tumor burden and lower Ki-67 positivity compared to controls (Fig. 2J). Notably, metastatic lesions were observed exclusively in *Krt19-cre^{+}Trp53$^{MT/MT}$Kras$^{G12D/+}$* mice with wildtype *Rest* expression, with no detectable metastases in *Rest*-deficient mice (Fig. 2J). These findings establish REST as a critical promoter of PDAC progression and metastasis.

3.3 REST Suppresses GSDMC-Dependent Pyroptosis to Promote PDAC Cell Survival

To investigate the mechanistic basis of REST-mediated PDAC progression, we first examined its role in regulating cell death pathways. REST knockdown significantly impaired PANC-1 and AsPC-1 cell viability, an effect that was partially rescued by either ROS scavengers or pan-caspase inhibitors (Fig. S2A-B), suggesting the involvement of pyroptosis. Subsequent characterization of gasdermin family members revealed that REST depletion specifically induced cleavage of GSDMC, but not other family members (GSDMA, GSDMB, GSDMD, or GSDME) in both cell lines (Fig. S2C). Importantly, the REST depletion-induced viability repression remained unaffected by inhibitors of apoptosis (Z-DEVD), necroptosis (NSA), or ferroptosis (Fer-1) (Fig. S2B), confirming the specific induction of GSDMC-dependent pyroptosis upon REST depletion.

Given the established role of caspase-8 in GSDMC-mediated pyroptosis and inflammatory cytokine processing, we systematically evaluated its activation across multiple experimental systems. Immunohistochemical analysis demonstrated marked upregulation of cleaved caspase-8 in pancreatic tumors from REST-deficient Krt19-cre+;KrasG12D/+ mice compared to controls (Fig. 3A). Western blot analysis of tumor lysates confirmed concurrent elevation of both GSDMC-N and cleaved caspase-8 in REST-depleted tumors (Fig. 3B). In vitro, REST depletion induced characteristic pyroptosis (Fig. 3C) and significantly increased both GSDMC and caspase-8 activation in PANC-1 cells (Fig. 3D-E).Detailed analysis of IL-1β and IL-18 processing revealed that REST knockdown specifically enhanced the maturation of these cytokines (Fig. 3F-G). To establish the functional dependency on GSDMC, we performed rescue experiments in REST-knockdown cells. Knockdown of GSDMC not only restored proliferative capacity and invasive potential (Fig. 3H-K, S2E-F), but also attenuated cell death, directly linking the pro-survival function of REST to suppression of GSDMC/caspase-8-mediated pyroptosis.

3.4 ROS-Mediated DR6 Activation in REST Knockdown-Induced Pyroptosis

Gene enrichment analysis revealed significant upregulation of ROS-associated genes in REST-knockdown PANC-1 and AsPC-1 cells, suggesting potential involvement of ROS in REST depletion-induced pyroptosis (Fig. S2B). Direct measurement confirmed increased intracellular ROS levels

following REST knockdown (Fig. 4B). This ROS dependence was further demonstrated by NAC (ROS inhibitor) treatment, which attenuated pyroptotic morphology and reduced cleavage of both GSDMC and caspase-8 in REST-silenced cells (Fig. 4C-E). NAC also significantly inhibited maturation and secretion of IL-1β and IL-18 in these cells (Fig. 4F-G). Together, these findings establish ROS as a critical mediator of pyroptosis induced by REST depletion.

Previous studies established that death receptor 6 (DR6) regulates caspase-8 activation through oxidation-dependent mechanisms(21). Our results showed that silencing DR6 attenuated pyroptosis induced by REST knockdown in PANC-1 and AsPC-1 cells, indicating that DR6 is critically involved in REST-mediated pyroptosis. (Figure S3A-C). Our experiments showed that ROS inhibition blocked REST knockdown-induced DR6 translocation (Fig. 4H-I). Consistent with reports that oxidized death receptor complexes are Triton X-100-resistant(22). We observed ROS-dependent accumulation of oxidized DR6 in the Triton X-100-insoluble fraction following REST depletion (Fig. 4J). Co-immunoprecipitation assays further revealed that NAC treatment disrupted the REST knockdown-induced interaction between DR6, caspase-8, and GSDMC (Fig. 4K). These findings collectively demonstrate that REST loss triggers ROS production, which activates DR6 to initiate pyroptosis through caspase-8/GSDMC signaling.

3.5 REST-Mediated Transcriptional Repression of NOXA1 Attenuates Pyroptosis in PDAC

To systematically investigate the molecular mechanisms by which REST regulates ROS production in PDAC, we performed comprehensive transcriptomic profiling of REST-deficient PANC-1 and AsPC-1 cells. Our RNA-seq analysis revealed significant upregulation of NADPH oxidase activator 1 (NOXA1), a critical regulator of ROS generation, upon REST knockdown (Fig. 5A). This finding was further substantiated by interrogation of TCGA and GTEx datasets, which demonstrated a robust inverse correlation between NOXA1 and REST mRNA expression levels across pancreatic cancer specimens (Fig. 5B and Fig. S4A). Importantly, immunohistochemical analysis of our PDAC tissue microarray confirmed this negative association at the protein level, with high REST expression correlating with diminished NOXA1 immunoreactivity (Fig. 5C).The REST-NOXA1 regulatory axis was further validated through multiple experimental approaches. Quantitative PCR and immunoblotting confirmed elevated NOXA1 expression in PANC-1(shREST) cells at both transcriptional and translational levels (Fig. 5D). In vivo studies using xenograft models and genetically engineered PDAC mice (Krt19-cre+;KrasG12D/+) with REST knockdown consistently showed reduced NOXA1 expression by IHC (Fig. 5E-F), establishing NOXA1 as a downstream target of REST in both cellular and animal models.

To elucidate the molecular basis of REST-mediated NOXA1 repression, we employed an integrated computational and experimental approach. JASPAR-based motif analysis identified a canonical RE-1 silencing element within the proximal promoter region (-2000 bp) of NOXA1(23). Chromatin immunoprecipitation assays demonstrated significant enrichment of REST at this RE-1 site in PANC-1 cells (Fig. 5G), suggesting direct transcriptional regulation. Functional validation through luciferase reporter assays revealed that REST overexpression significantly attenuated NOXA1 promoter activity,

while deletion of the RE-1 element completely abolished this repressive effect (Fig. 5H). Nuclear run-on assays provided additional mechanistic insight, showing that REST binding substantially decreased the transcription initiation rate of NOXA1 (Fig. 5I), confirming REST's role as a direct transcriptional repressor of NOXA1.

To establish the functional consequences of this regulatory relationship, we performed rescue experiments in REST-deficient PDAC cells. NOXA1 knockdown in REST-silenced PANC-1 and AsPC-1 cells significantly attenuated intracellular ROS accumulation (Fig. 5J) and markedly reduced the proteolytic activation of both GSDMC and caspase-8 (Fig. 5K). Furthermore, NOXA1 inhibition substantially diminished the maturation and secretion of the proinflammatory cytokines IL-1β and IL-18 (Fig. 5L), key mediators of pyroptosis. Functional assays demonstrated that NOXA1 silencing not only rescued the proliferative, invasive, and colony-forming capacities of REST-deficient cells but also significantly reduced cell death (Fig. S4B-G). Collectively, these findings establish a novel REST-NOXA1-ROS signaling axis that critically regulates pyroptosis in PDAC, with important implications for therapeutic targeting of this pathway.

3.5 Targeting REST inhibits PDAC progression

To evaluate the therapeutic potential of REST inhibition in PDAC, we developed an AAV8 vector encoding REST-targeting shRNA (AAV8-shREST) (Fig.S5A). Functional assays demonstrated that AAV8-shREST treatment significantly impaired PANC-1 cell proliferation, as evidenced by both MTS and BrdU incorporation assays (Fig. 6A-B). Importantly, REST inhibition sensitized PANC-1 cells to paclitaxel-induced cytotoxicity, as shown by increased LDH release and TUNEL-positive cells (Fig. 6C-D).We next employed a 3D tumor spheroid model to validate these findings. AAV8-shREST treatment for 7 days significantly suppressed PANC-1 spheroid growth compared to control (AAV8-shCTL) treatment (Fig. 6E). This anti-tumor effect was further confirmed in PANC-1 patient-derived xenograft (PDX) models, where AAV8-shREST administration substantially reduced tumor growth and decreased Ki-67 expression (Fig. 6F).

To assess the therapeutic efficacy in a genetically engineered mouse model, we administered AAV8-shREST to Krt19-cre+;KrasG12D/+ mice (Fig. 6G). Successful pancreatic ductal cell-specific REST knockdown was verified (Fig. S5B-C). AAV8-shREST treatment conferred significant survival benefits compared to control and reduced tumor burden, as demonstrated by decreased tumor weight, lower Ki-67 positivity, and reduced metastatic incidence (Fig. 6H). These results collectively demonstrate that therapeutic REST targeting suppresses PDAC progression and metastasis, potentially through induction of pyroptosis, highlighting its clinical translational potential.

4. DISCUSSION

In the present study, we provided evidences suggesting that REST is an oncogene of PDAC via inhibiting ROS-mediated pyroptosis, which adds to its multiple functions in regulating cell development and disease. We demonstrated that REST repressed the NOXA1 expression, which is known for its role in

promoting ROS production. Mechanistically, REST was recruited to the RE-1 element in NOXA1 gene promotor and repressed NOXA1 gene transcription. Increased ROS induced by NOXA1 promotes oxidation of DR6 and subsequently recruits Caspase-8 and GSDMC for the cleavage of GSDMC by active Caspase-8, thereby inducing pyroptosis. Importantly, this study identified a previously unreported signal transduction pathway for inducing PDAC cell pyroptosis by targeting REST, which would be a proper way for inhibiting PDAC oncogenesis, progression, and metastasis.

Recent studies have highlighted the potential of inducing pyroptosis as a therapeutic strategy in PDAC. For instance, chemotherapy agents such as gemcitabine have been shown to induce GSDME-mediated pyroptosis in PDAC cells, although GSDME expression is often low in tumor cells (30). Similarly, other studies have reported that targeting the inflammasome pathway can trigger GSDMD-dependent pyroptosis in pancreatic cancer (13). However, these pathways are frequently suppressed in advanced PDAC due to acquired resistance mechanisms. Our study identifies GSDMC as a key executor of pyroptosis in PDAC, which is distinct from the previously reported GSDMD- or GSDME-dependent mechanisms. Importantly, we demonstrate that REST acts as a master repressor of GSDMC-mediated pyroptosis by transcriptionally silencing NOXA1, thereby attenuating ROS production and DR6 oxidation. This finding positions the REST-NOXA1-ROS axis as a previously unrecognized checkpoint controlling GSDMC-dependent pyroptosis in PDAC.

REST has been extensively studied as a transcriptional repressor in neuronal development and is known to function as a tumor suppressor in several epithelial cancers, including breast and prostate cancer(24–26). In these contexts, loss of REST promotes neuroendocrine differentiation and aggressive tumor behavior. In contrast, our findings reveal an oncogenic role for REST in PDAC, where it promotes tumor progression by suppressing pyroptosis. This context-dependent duality may be explained by the unique cellular origin of PDAC, which arises from acinar-to-ductal metaplasia which was distinct from the epithelial-to-mesenchymal transition observed in other cancers(6). REST is specifically expressed in adult ductal cells but not in acinar or endocrine cells of the pancreas (10, 11), suggesting that REST may be required to establish and maintain the ductal phenotype during metaplasia. In this context, REST-mediated suppression of pyroptosis could represent a protective mechanism that allows transdifferentiating cells to survive metabolic stress. However, in malignant PDAC, this same pathway is associated with tumor progression by enabling cells to evade programmed cell death. Thus, REST's function as an oncogene or tumor suppressor likely depends on the differentiation state and cellular lineage of the cancer, highlighting the importance of cell context in determining transcriptional repressor functions.

Uncontrolled ROS production played critical roles in pyroptosis(27, 28). Our results showed that REST depletion increased the ROS production in PDAC cells and ROS inhibitor NAC attenuated the effect of REST knockdown on PDAC progression inhibition and the activation of Caspase-8(Fig. 3). Uncontrolled production of ROS was associated with alteration of NADH oxidases(29).Our research revealed that the NOXA1 gene acts as a downstream target for REST, with REST directly attaching to the NOXA1 gene's promoter, leading to a subsequent suppression of NOXA1 gene transcription (Fig. 4). While we cannot

rule out the involvement of additional NADH oxidases in this mechanism, our findings clearly indicate that specific silencing of NOXA1 counteracts the upregulation of ROS and the cell pyroptosis resulting from the depletion of REST (Fig. 4). These data suggested NOXA1 mediated ROS production is crucial in REST depletion induced cell pyroptosis.

The majority of current researches have focused on the activation modes of GSDME. However, it has been reported that GSDME is merely expressed in most tumor cells but is highly expressed in normal cells, which leads to pyroptosis of normal tissues other than tumor cells upon the administration of chemotherapeutic drugs(30). Identifying other gasdermin family members that participated in tumor pyroptosis is of great importance. Our results illustrated that loss-of REST induced ROS production could promote GSDMC cleavage to induce pyroptosis, suggesting targeting REST may specific induced pyroptosis of tumor. During this process, active Caspase-8 would not release into the cytosol which will cause cleavage of widespread cytosolic proapoptotic substrates, such as pro-caspase-3 and Bid. Instead, the DR6/GSDMC/Caspase-8 complex would enable direct GSDMC cleavage by active Caspase-8. These results suggested that REST depletion specifically initiated pyroptosis but not apoptosis in PDAC cells which was supported by the results that it is pyroptosis inhibitor but not apoptosis inhibitor alleviated the PDAC cell death induced by REST loss.

Targeting REST to induce GSDMC-mediated pyroptosis offers a dual therapeutic strategy: direct tumor killing and sensitization to chemotherapy by overcoming apoptosis resistance. The accompanying release of proinflammatory cytokines could also enhance responses to immune checkpoint blockade. While AAV8-mediated REST knockdown shows preclinical promise, clinical translation will require optimized delivery to tumors, safety validation in normal tissues, and biomarkers for patient selection.

Collectively, our research offers evidence that the overexpression of REST in human PDAC could significantly contribute to the development of a more advanced and poorly prognostic phenotype. Targeting REST to induce GSDMC-mediated pyroptosis represents a novel therapeutic strategy for PDAC that combines direct antitumor effects.

Declarations

Ethics approval and consent to participate

All procedures were approved by the research ethics committee of The Second Affiliated Hospital of Dalian Medical University (Certificate No. 2020 No.120). All patients included in this research have signed the consents.

Consent for publication

All authors of the manuscript have read and agreed to its content and are accountable for all aspects of the accuracy and integrity of the manuscript in accordance with ICMJE criteria. The manuscript or

portions thereof are not under consideration by any other journal, that these findings have not been previously published.

Competing interests

The authors declared they do not have anything to disclose regarding conflict of interest with respect to this manuscript.

Funding

This work is supported by the Basic Research Projects of Liaoning Provincial Department of Education (LJKMZ20221291 to Sui C) and Scientific Research Project of Pudong New Area Science and Economic Commission (PKJ2022-Y18), Key Discipline Construction Project Pudong Health Bureau of Shanghai (PWZxk2022-02), Academic Leaders Training Program of Pudong Health Bureau of Shanghai (PWRd2022-05).

Availability of data

The data that support the findings of this study are available from the corresponding author upon reasonable request.

Patient consent for publication

Not applicable

Author Contribution

Concept and design: Sui C, Li M, Li R

Acquisition of data: Sui C, Li J

Analysis and interpretation of data: Sui C, Li J

Drafting the manuscript: Sui C, Li J

Critical revision of the manuscript: Li M, Li R

Statistically analysis: Sui C, Li J

Obtain funding: Li J,Li M

Administrative, technical, or material support: Li J

Acknowledgements

Not applicable

References

1. Siegel, R.L.*, et al.* (2019) Cancer statistics, 2019. *CA Cancer J Clin*, **69**, 7-34.
2. Mizrahi, J.D.*, et al.* (2020) Pancreatic cancer. *Lancet*, **395**, 2008-2020.
3. Kleeff, J.*, et al.* (2016) Pancreatic cancer. *Nat Rev Dis Primers*, **2**, 16022.
4. Hsu, S.K.*, et al.* (2022) The Role of Nonapoptotic Programmed Cell Death - Ferroptosis, Necroptosis, and Pyroptosis - in Pancreatic Ductal Adenocarcinoma Treatment. *Front Oncol*, **12**, 872883.
5. Quinonero, F.*, et al.* (2019) The challenge of drug resistance in pancreatic ductal adenocarcinoma: a current overview. *Cancer Biol Med*, **16**, 688-699.
6. Storz, P. (2017) Acinar cell plasticity and development of pancreatic ductal adenocarcinoma. *Nat Rev Gastroenterol Hepatol*, **14**, 296-304.
7. Rovira, M.*, et al.* (2021) REST is a major negative regulator of endocrine differentiation during pancreas organogenesis. *Genes Dev*, **35**, 1229-1242.
8. Schoenherr, C.J.*, et al.* (1995) The neuron-restrictive silencer factor (NRSF): a coordinate repressor of multiple neuron-specific genes. *Science*, **267**, 1360-3.
9. Baldelli, P.*, et al.* (2015) The Transcription Repressor REST in Adult Neurons: Physiology, Pathology, and Diseases. *eNeuro*, **2**.
10. Tabula Muris, C.*, et al.* (2018) Single-cell transcriptomics of 20 mouse organs creates a Tabula Muris. *Nature*, **562**, 367-372.
11. de la, O.S.*, et al.* (2023) Single-cell chromatin accessibility of developing murine pancreas identifies cell state-specific gene regulatory programs. *Mol Metab*, **73**, 101735.
12. Shi, J.*, et al.* (2017) Pyroptosis: Gasdermin-Mediated Programmed Necrotic Cell Death. *Trends Biochem Sci*, **42**, 245-254.
13. Bergsbaken, T.*, et al.* (2009) Pyroptosis: host cell death and inflammation. *Nat Rev Microbiol*, **7**, 99-109.
14. Shi, J.*, et al.* (2015) Cleavage of GSDMD by inflammatory caspases determines pyroptotic cell death. *Nature*, **526**, 660-5.
15. Stienstra, R.*, et al.* (2010) The inflammasome-mediated caspase-1 activation controls adipocyte differentiation and insulin sensitivity. *Cell Metab*, **12**, 593-605.
16. Cieniewicz, B.*, et al.* (2015) Murine Gammaherpesvirus 68 Pathogenesis Is Independent of Caspase-1 and Caspase-11 in Mice and Impairs Interleukin-1beta Production upon Extrinsic Stimulation in Culture. *J Virol*, **89**, 6562-74.
17. Tang, Z.*, et al.* (2017) GEPIA: a web server for cancer and normal gene expression profiling and interactive analyses. *Nucleic Acids Res*, **45**, W98-W102.
18. Hoadley, K.A.*, et al.* (2018) Cell-of-Origin Patterns Dominate the Molecular Classification of 10,000 Tumors from 33 Types of Cancer. *Cell*, **173**, 291-304 e6.

19. Yang, S.*, et al.* (2016) A Novel MIF Signaling Pathway Drives the Malignant Character of Pancreatic Cancer by Targeting NR3C2. *Cancer Res*, **76**, 3838-50.
20. Moffitt, R.A.*, et al.* (2015) Virtual microdissection identifies distinct tumor- and stroma-specific subtypes of pancreatic ductal adenocarcinoma. *Nat Genet*, **47**, 1168-78.
21. Zhang, J.Y.*, et al.* (2021) The metabolite alpha-KG induces GSDMC-dependent pyroptosis through death receptor 6-activated caspase-8. *Cell Res*, **31**, 980-997.
22. Legler, D.F.*, et al.* (2003) Recruitment of TNF receptor 1 to lipid rafts is essential for TNFalpha-mediated NF-kappaB activation. *Immunity*, **18**, 655-64.
23. Wasserman, W.W.*, et al.* (2004) Applied bioinformatics for the identification of regulatory elements. *Nat Rev Genet*, **5**, 276-87.
24. Li, Y.*, et al.* (2017) SRRM4 Drives Neuroendocrine Transdifferentiation of Prostate Adenocarcinoma Under Androgen Receptor Pathway Inhibition. *Eur Urol*, **71**, 68-78.
25. Wagoner, M.P.*, et al.* (2010) The transcription factor REST is lost in aggressive breast cancer. *PLoS Genet*, **6**, e1000979.
26. Cloud, A.S.*, et al.* (2022) Loss of the repressor REST affects progesterone receptor function and promotes uterine leiomyoma pathogenesis. *Proc Natl Acad Sci U S A*, **119**, e2205524119.
27. An, H.*, et al.* (2021) Tetraarsenic hexoxide enhances generation of mitochondrial ROS to promote pyroptosis by inducing the activation of caspase-3/GSDME in triple-negative breast cancer cells. *Cell Death Dis*, **12**, 159.
28. Zhou, B.*, et al.* (2018) Tom20 senses iron-activated ROS signaling to promote melanoma cell pyroptosis. *Cell Res*, **28**, 1171-1185.
29. Niu, X.L.*, et al.* (2010) Nox activator 1: a potential target for modulation of vascular reactive oxygen species in atherosclerotic arteries. *Circulation*, **121**, 549-59.
30. Ouyang, X.*, et al.* (2023) Pyroptosis, inflammasome, and gasdermins in tumor immunity. *Innate Immun*, **29**, 3-13.

Figures

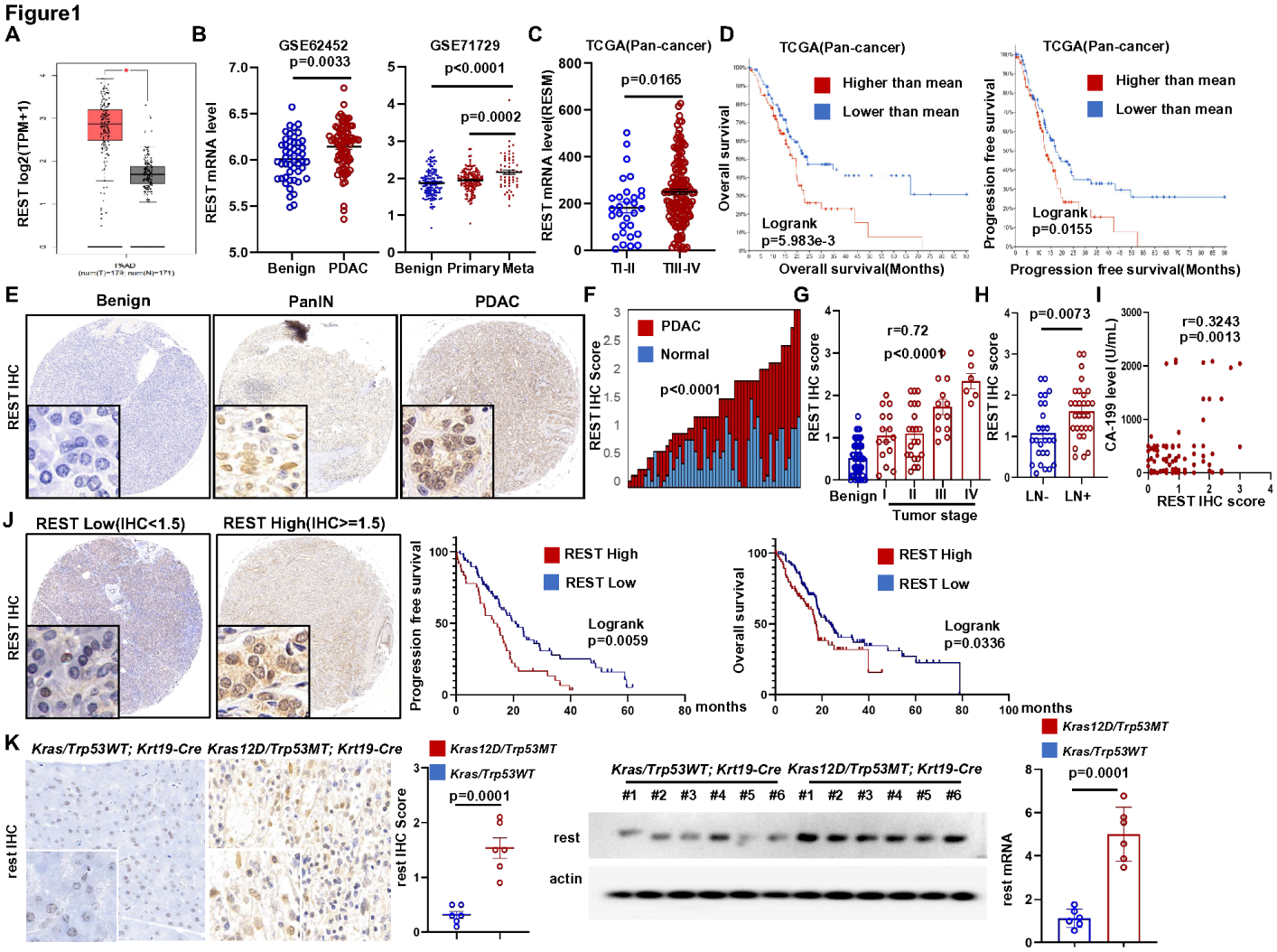


Figure 1

REST is overexpressed in PDAC tissues derived from human and animal model

A) RNA-seq data from GTEx database were analyzed using GEPIA software (http://gepia.cancer-pku.cn/). REST mRNA levels were compared between benign pancreatic ductal tissue and pancreatic tumors. **B)** RNA-seq analyses (GSE62452 and GSE71729) compared REST mRNA levels among benign pancreatic tissue, primary pancreatic ductal tumors, and metastatic pancreatic ductal tumors. **C-D)** RNA-seq data from TCGA database were analyzed using cbioportal software (http://www.cbioportal.org/), C) REST mRNA levels were compared among different tumor stages, D) Z-scores were used to divide PDAC patients into REST low and high groups. Kaplan-Meier curves plot overall survival and disease-free survival of PDAC patients by REST expression. **E)** Representative IHC staining for REST on the Benigh-PDAC TMA showing primary healthy tissue, PanIN, and primary PDAC. **F)** Plot of REST IHC score comparing PDAC and adjacent healthy tissue. **G)** Scattered plots show REST IHC scores of indicated tumor groups. The association of REST expression with tumor stage was calculated by Spearman's correlation test. **H)** Scattered plots show REST IHC scores distribution in tumor with or without

lymphnodes metastasis. **I)** Correlation of serum CA-199 level with REST IHC scores was calculated by Persson's correlation test. **J)** IHC staining for REST on the PDAC-survival TMA were performed and IHC-scores were used to divide PDAC patients into REST low and high groups. Kaplan-Meier curves plot overall survival and progression-free survival of PDAC patients by in different groups. **K)** PDAC animal models were generated as described in the M&M section. Immunohistochemical analysis of REST protein expression in 3-mo-old *Krt19-cre^{+}Trp53$^{WT/WT}$Kras$^{WT/WT}$* or *Krt19-cre^{+}Trp53$^{MT/MT}$Kras$^{G12D/+}$*. Total RNA and protein of pancreas of mice models were isolated, expression level of REST protein and mRNA were measured by immunoblotting and realtime-qPCR.

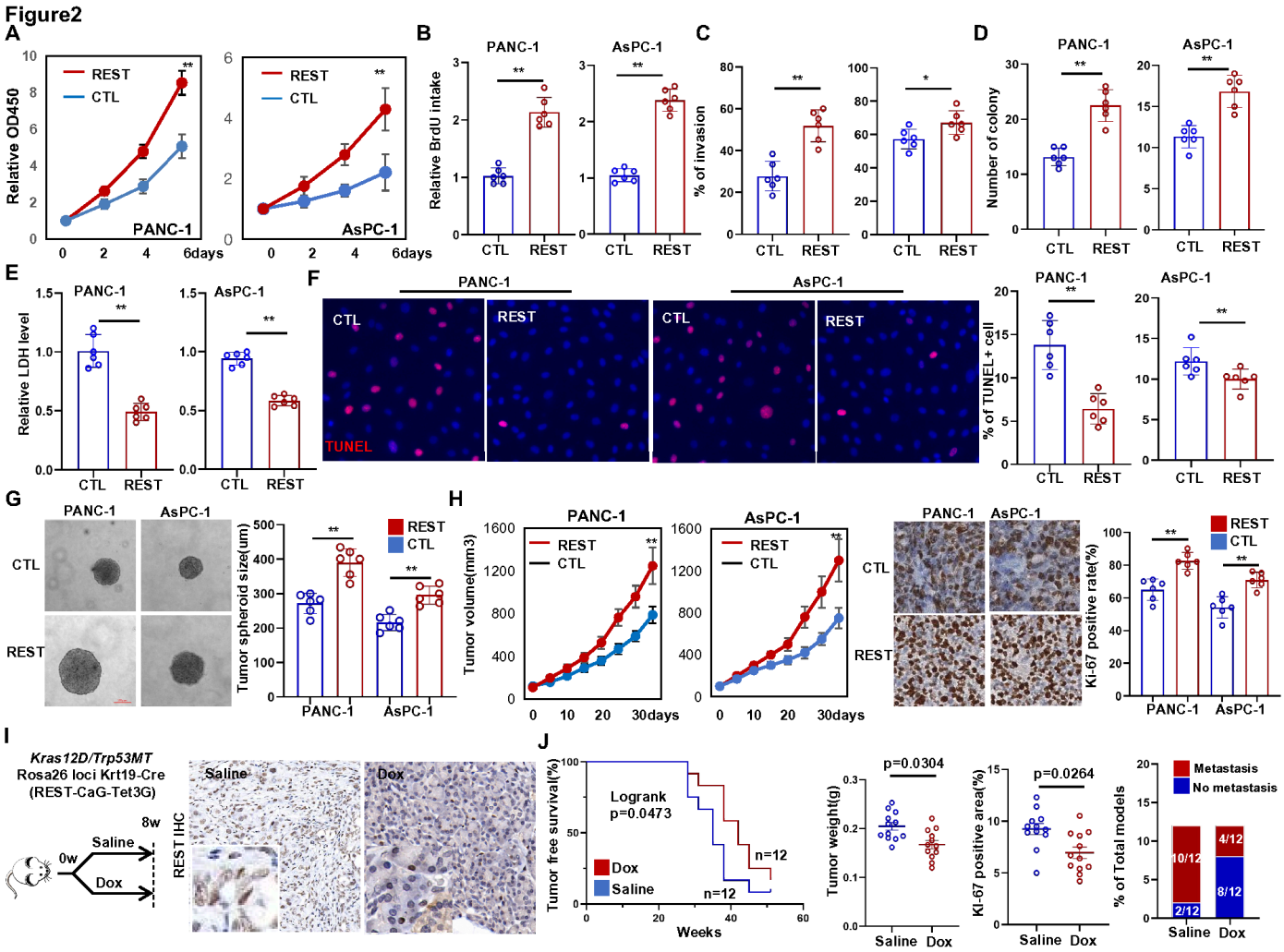


Figure 2

REST promotes PDAC cell proliferation and tumor growth

A-G) Gain-of-function of REST with was applied to PANC-1 and AsPC-1 cells. A) Cell proliferation was measured by MTS assays and presented as relative OD490 fold change to that at day 0. B) Relative BrdU incorporation rates were present. C) Cell invasion rates were measured by trans-well assays. D) Colony

formation assays were performed, and colony numbers were counted if their diameters were >100 um. E) LDH release were determined. F) TUNEL (red) positive cells rates were calculated. **G)** PANC-1 and AsPC-1 cells were cultured to generate 3D multi-cellular spheroids as described in the M&M section. Spheroids images were presented and Spheroids size changes were measured. **H)** PANC-1 and AsPC-1 xenografts were established as described in the Methods section. Tumor volumes were measured twice a week and plotted. Xenografts were collected at endpoint. IHC assays were performed to measure Ki-67 expression. Represented images were shown. **I)** The transgenic *Trp53*$^{MT/MT}$*Kras*$^{G12D/+}$ mice with pancreatic epithelial cell -specific knock down of the Rest gene induced by DOX were constructed as described in the Material and Methods. **J)** Kaplan-Meier analysis reveals an increased tumor-free survival in *Trp53*$^{MT/MT}$*Kras*$^{G12D/+}$ mice treated with DOX (n=12), significantly longer than the *Trp53*$^{MT/MT}$*Kras*$^{G12D/+}$ mice treated with saline (n=12). Knock down of Rest significantly decreased tumor weight, Ki-67 expression and tumor metastasis in *Trp53*$^{MT/MT}$*Kras*$^{G12D/+}$ mice model.

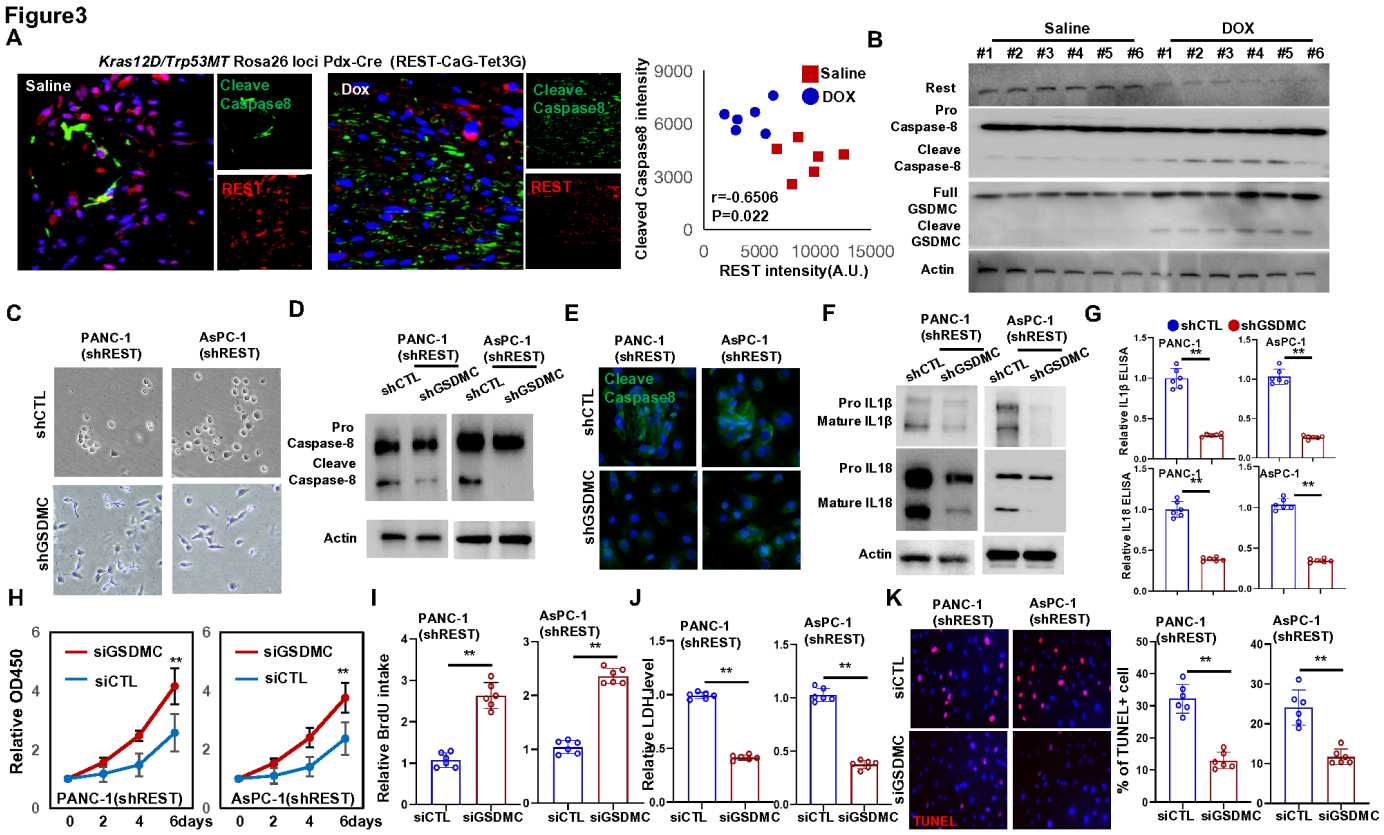


Figure 3

REST promotes PDAC progression via suppressing GSDMC-mediated cell pyroptosis

A-B) PDAC tumors derived from *Krt19-cre*$^{+}$*Trp53*$^{MT/MT}$*Kras*$^{G12D/+}$mice with or without DOX treatment were collected. A) Represented images of immunofluorescent staining using REST and cleaved Caspase-8 antibodies were shown. Association of REST and cleaved caspase-8 immunofluorescent intensity was calculated using Pearsons' correlation. B) Protein level of cleaved GSDMC and Caspase-8

using immunoblotting. **C)** Reduced pyroptotic morphology in PANC-1(shREST) and AsPC-1(shREST) cells following GSDMC knockdown. **D)** Protein level of cleaved GSDMC and Caspase-8 in PANC-1(shREST) and AsPC-1(shREST) cells were measured by immunoblotting. **E)** Immunofluorescent staining using cleaved Caspase-8 antibody was performed on PANC-1(shREST) and AsPC-1(shREST) cells with or without GSDMC knockdown. Represented images were shown. **F)** Immunoblot analysis showing different forms of IL1β and IL18 expression from PANC-1(shREST) and AsPC-1(shREST) cells with or without GSDMC knockdown. **G)** Secreted IL-1β and IL18 level in ANC-1(shREST) and AsPC-1(shREST) cells with or without GSDMC knockdown were measured by ELISA. **H-K)** PANC-1(shREST) and AsPC-1(shREST) with or without GSDMC knockdown were cultured and H) Cell proliferation was measured by MTS assays. I) Relative BrdU incorporation rates were present. J) LDH release were determined. K) TUNEL positive cells rates were calculated.

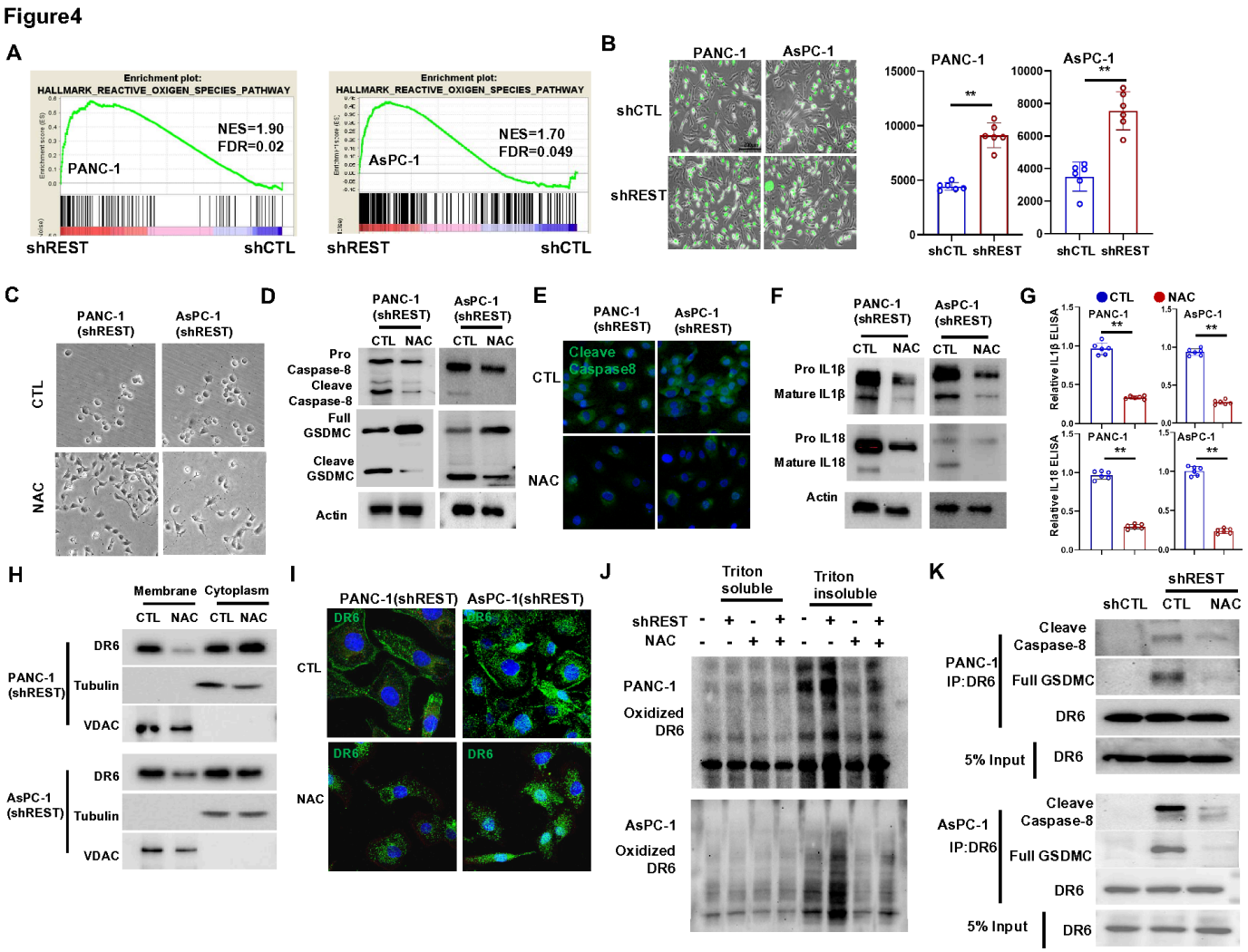


Figure 4

REST suppresses cell pyroptosis by inhibiting ROS production

A) GSEA analyses showed PANC-1 and AsPC-1 cells transcriptome with REST depletion have enrichments of ROS pathway associated genes. **B)** ROS production of PANC-1 and AsPC-1 with or without REST knockdown were measured and represented images were shown. **C)** ROS inhibitor (NAC) treatment reduced pyroptotic morphology in PANC-1(shREST) and AsPC-1(shREST) cells. **D-I)** PANC-1(shREST) and AsPC-1(shREST) cells were treated with vehicle or NAC. D) protein level of cleaved GSDMC and Caspase-8 were measured by immunoblotting. E) Immunofluorescent staining of cleaved Caspase-8 was performed and represented images were shown. F) Immunoblot analysis showing different forms of IL1β and IL18 expression. G) Secreted IL-1β and IL18 level were measured by ELISA. H) Cytoplasmic and membrane fractions were extracted. Membrane fraction marker VDAC, cytoplasmic fraction marker tubulin and DR6 was measured by immunoblotting. I) Immunofluorescence analysis showed that NAC treatment reduced the plasma membrane levels of DR6. **J-K)** PANC-1(shREST) and AsPC-1(shREST) were treated with or without NAC. J) The Tritox-X soluble and insoluble fraction were collected and used to detect oxidation of DR6. K) Total protein were collected and used to perform immunoprecipitation assays with the DR6 antibody. The associated proteins were detected by Caspase-8 and GSDMC antibodies.

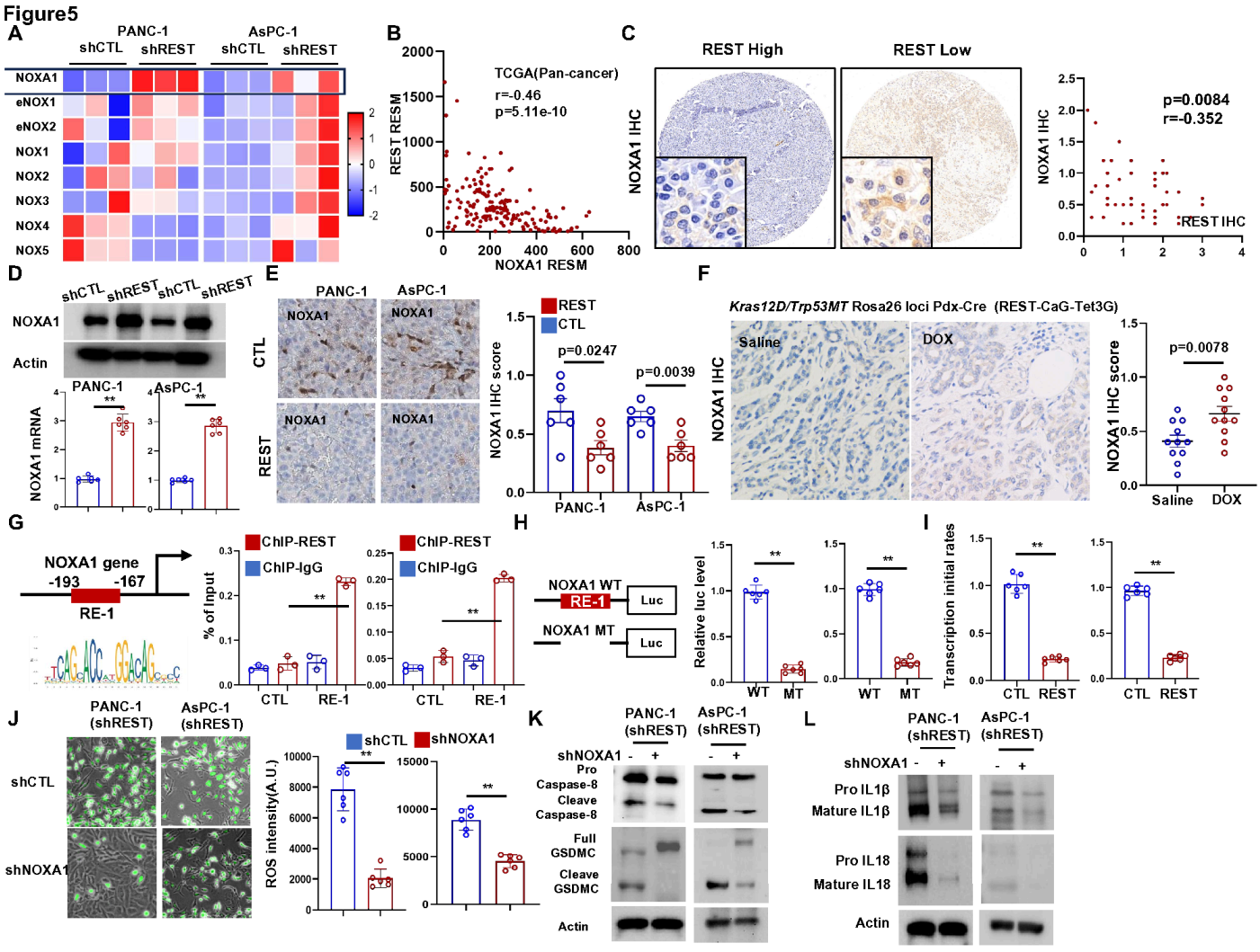


Figure 5

REST repressed NOXA1 gene transcription

A) RNA-seq results of ROS associated enzymes in PANC-1(shREST) and AsPC-1(shREST) cells. **B)** Negative association between REST and NOXA1 mRNA level in TCGA databases were presented. **C)** The NOXA1 IHC assays were performed on the survival-TMA as described in the Methods section. Representative images of NOXA1 IHC staining are shown. Scattered plots show NOXA1 IHC scores of indicated tumor groups. The association of NOXA1 expression with REST IHC scores was calculated by Person's correlation test. **D)** Increased NOXA1 mRNA and protein levels were detected in PANC-1 and AsPC-1 cells with REST knockdown. **E)** . Representative images of the NOXA1 IHC staining on PANC-1 and AsPC-1 xenografts were shown. **F)** The transgenic $Trp53^{MT/MT}Kras^{G12D/+}$ mice with pancreatic epithelial cell -specific knockdown of the REST gene induced by DOX were constructed as described in the Material and Methods section. IHC assays were performed to measure NOXA1 expression. Represented images were shown. **G)** RE-1 elements in NOXA1 gene were predicted using JASPAR software and binding site was showed in the schematic diagrams. PANC-1 and AsPC-1 cells were used to perform ChIP assays with the Flag or IgG antibodies. Signals were calculated as the percentage of input. **H)** PANC-1 and AsPC-1 cells were co-transfected with REST and wild type(WT) or RE-1 deleted(MT) NOXA1-Luc vectors. Luciferase assays were performed. **I)** PANC-1 and AsPC-1 with or without REST overexpression were used to perform RNA run-on assays. Nascent NOXA1 mRNAs were measured by real-time qPCR. **J-L)** PANC-1(shREST) and ASPC-1(shREST) cells were transcribed with vectors encoding either control shRNA of shRNA targeting NOXA1. J) ROS production was measured and represented images were shown. Representative immunoblot analysis showing K) different forms of IL1β and IL18 expression from and L) cleaved Caspase-8 and GSDMC in indicated cells.

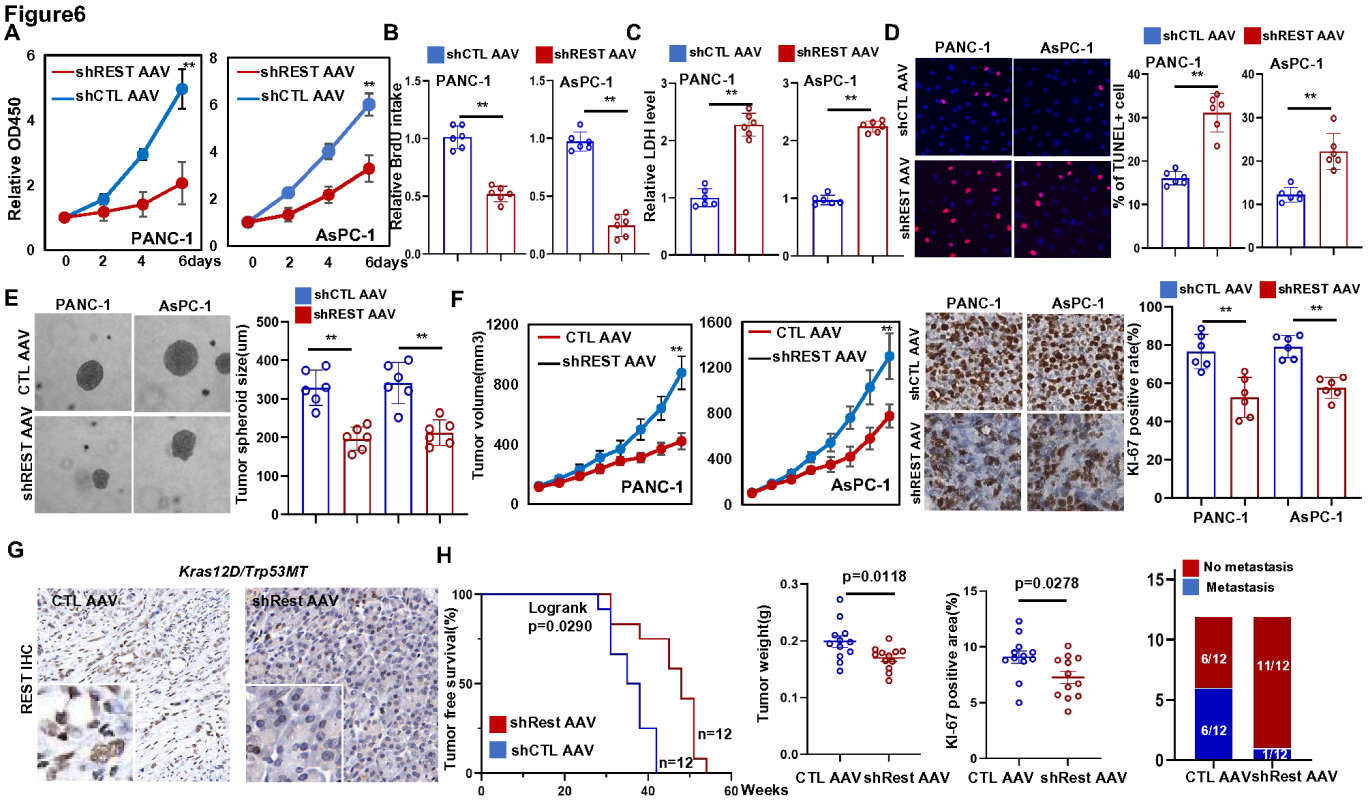


Figure 6

Targeting REST repressed PDAC cell proliferation and tumor growth

A-F) AAV-shREST specifically targeting pancreatic ductal epithelial cells was generated as described in Material and Methods section and used to transduce PANC-1 and AsPC-1 cell lines. A) Cell proliferation rates were measured by MTS assays. B) Relative BrdU incorporation rates were present. C) LDH release were determined. D) TUNEL positive cells rates were calculated. E) PANC-1 and AsPC-1 cell spheroids size changes were measured. F) PANC-1 and AsPC-1 xenografts were established and treated with AAVs. Tumor volumes were plotted. IHC assays were performed to measure Ki-67 expression. **G)** *Krt19-cre*$^{+}$*Trp53*$^{MT/MT}$*Kras*$^{G12D/+}$ Mice (n=12 per group) received retrograde intraductal infusion of 4×10^{12}vg/kg control AAV or AAV-shREST. **H)** Kaplan-Meier analysis demonstrated prolonged tumor-free survival in mice treated with AAV-shREST. Knockdown of REST significantly reduced tumor burden, Ki-67 expression, and metastatic incidence.

Supplementary Files

This is a list of supplementary files associated with this preprint. Click to download.

- Graphticabstract.pdf

- RESTPAAD20260423WB.pdf
- Supplementarytable1.xlsx
- Supplementarytable2.xlsx
- fig7.png
- fig8.png
- fig9.png
- fig10.png
- fig11.png